24th International Conference on Renewable Energies and Power Quality (ICREPQ'26)
Santander (Spain), 10th to 12th June 2026
ISBN-13: 978-84-09-82044-3

Enhanced distance-protection algorithm for accurate fault location and resistance characterization under double phase-to-ground conditions

I. San Sebastian[1,2], Marene Larruskain[1], Felipe Uriondo[1] and Itxaso Aranzabal[1]

[1] Department of Electrical Engineering
UPV/EHU University of the Basque Country
School of Engineering Bilbao. Plaza Ingeniero Torres Quevedo, 1, 48013-Bilbao, Spain
[2] INGETEAM.Power Technology
Parque Tecnológico de Bizkaia, Ed.700, 48170, Zamudio, Spain

Abstract. The distance-protection function is employed to safeguard high-voltage transmission lines against single-phase, double-phase, double phase-to-ground, and three-phase faults. In radial systems, or in double-end-fed configurations with homogeneous networks where the line is protected from the strong source end, the accuracy of conventional distance protection methods is inherently constrained. This paper presents a robust solution for accurately estimating the fault distance during double phase-to-ground faults as well as the fault resistances. The algorithm considers two scenarios. One for equal fault resistances in the two involved phases, a condition that keeps the sequence networks decoupled and permits the use of sequence-domain measurements. The other scenario involves unequal phase fault resistances, which couple the sequence networks and therefore require phase-domain voltage and current measurements. Together, these cases cover the full range of resistance configurations, ensuring a thorough and reliable proposed approach. The algorithm is validated with simulations and a real field fault case.

Key words. Distance Protection, Fault Location, Fault Resistance.

A, B, C	Consecutive phases of a three-phase system.
0,1,2	Zero, positive, and negative sequence components of the three-phase system.
V	Voltage phasor.
I	Current phasor.
Δ	Difference between fault and prefault conditions.
a	Complex operator. Its value is $1\angle 120°$.
R_{FA}	Fault resistance of phase A.
R_{FB}	Fault resistance of phase B.
R_{FC}	Fault resistance of phase C.
R_G	Ground fault resistance.
L	Length of the protected line.
$\mathbf{Z_S}$	Self-impedance of the phase.
$\mathbf{Z_M}$	Mutual impedance of the phase.
$\mathbf{Z_L}$	Line impedance.
p	Fault distance in per-unit values.
d	Fault distance in kilometers.

1. Introduction

The distance-protection function is widely used to protect high-voltage transmission lines against different faults [1-3]. In radial networks, as well as in double-end-fed systems with homogeneous line parameters where protection is applied from the strong-source end, this function exhibits a high degree of accuracy for single-phase, double-phase, and three-phase faults [4][5], even when significant fault resistances are present [6][7]. Under these conditions, the positive, negative, and zero-sequence components remain sufficiently predictable to ensure a reliable estimation of the apparent impedance seen by the relay [8][9].

For double phase-to-ground faults, however, the situation becomes more complex [10]. The loops used to estimate the fault distance and the associated fault resistances correspond to the single-phase and double phase loops [11-13]. The interaction between these loops is influenced by the resistive components of the two faulted phases and by the ground resistance [14]. As a result, the apparent impedance measured by the relay may deviate substantially from the real one, reducing the accuracy of conventional distance-protection methods [15][16].

This dependence on the distribution of fault resistances often leads to estimation errors that vary notably with system conditions, fault location, and the relative magnitudes of phase and ground resistances [17][18]. Previous research has attempted to mitigate resistance-induced errors using compensation factors [19] [20], however, these approaches often fail when phase resistances are unbalanced [21].

Furthermore, there is a lack of unified methodologies capable of accurately addressing both balanced and unbalanced fault resistance scenarios within a single analytical framework. Existing solutions typically focus on either sequence-domain formulations, which lose validity under coupled conditions, or phase-domain approaches that do not explicitly exploit the structure of the sequence networks when decoupling is present. This gap highlights the need for a flexible and robust method that can adapt its formulation depending on the fault resistance configuration while maintaining high accuracy in fault distance estimation. In this context, the main novelty of this work lies in the development of a dual-domain approach that systematically handles both decoupled and coupled sequence network conditions, enabling reliable distance protection performance across a wider range of realistic fault scenarios.

To address these limitations, this paper introduces a robust methodology capable of accurately determining the fault distance in the presence of double phase-to-ground faults. The proposed approach enhances the interpretation of voltage and current quantities under unbalanced and resistive fault scenarios, improving the reliability of the distance estimation even when traditional loop models become inaccurate.

The algorithm considers two scenarios. In the first scenario, the fault resistances of the two involved phases have the same value. Under these conditions, the sequence networks remain decoupled, and the analysis is performed using sequence voltage and current measurements. In the second scenario, the fault resistances of the two phases differ, resulting in coupled sequence networks. Consequently, phase-domain voltage and current measurements are required.

The paper is organized into four sections, including this introduction. Section 2 introduces fault-distance calculation for decoupled and coupled sequence networks. Section 3 validates the proposed algorithm with simulations, as well as a real field fault. Finally, Section 4 concludes the paper and discusses the practical applicability of the proposed solution.

2. Fault-distance calculation

This section details the development of the equations used to determine the fault distance and the fault resistances.

A. Primary scheme

Fig. 1 illustrates the primary scheme of a double phase-to-ground fault, corresponding to a *BC* phase-to-ground (*BCG*) faults. $\mathbf{V_A}$

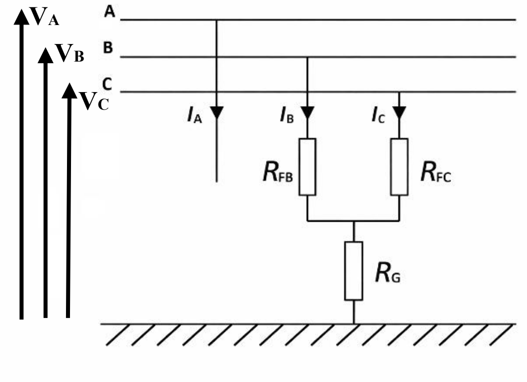

Fig. 1. *BCG* fault.

B. Fault distance calculation with decoupled sequence networks

For the sequence networks to remain decoupled during a *BCG* double phase-to-ground fault, the fault resistances in the affected phases, *B*-phase (R_{FB}) and *C*-phase (R_{FC}) must be equal, as shown in (1).

$$R_{FB} = R_{FC} \tag{1}$$

Under this condition, the three sequence networks are connected in parallel. Fig. 2 represents the same fault case as Fig. 1, expressed through decoupled sequence networks.

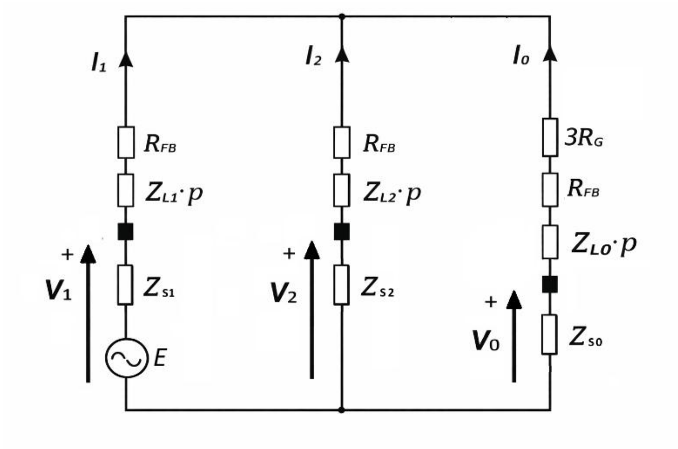

Fig. 2. Sequence network for a *BCG* fault under decoupled conditions.

The equations involved are shown in (2):

$$\mathbf{V_1} - \mathbf{I_1} \cdot p \cdot \mathbf{Z_{L1}} - \mathbf{I_1} \cdot R_{FB} = \boldsymbol{V_2} - \mathbf{I_2} \cdot p \cdot \mathbf{Z_{L2}} - \mathbf{I_2} \cdot R_{FB}$$

$$\begin{aligned}\mathbf{V_0} - \mathbf{I_0} \cdot p \cdot \mathbf{Z_{L0}} - \mathbf{I_0} \cdot R_{FB} - \mathbf{I_0} \cdot 3R_G \\ = \mathbf{V_2} - \mathbf{I_2} \cdot p \cdot \mathbf{Z_{L2}} - \mathbf{I_2} \cdot R_{FB}\end{aligned}$$

$$\mathbf{Z_{L1}} = \mathbf{Z_{L2}} \tag{2}$$

where:
$\mathbf{V_1}$, $\mathbf{V_2}$ and $\mathbf{V_0}$ are the positive-, negative- and zero-sequence voltage of phase *A*;
$\mathbf{I_1}$, $\mathbf{I_2}$, and $\mathbf{I_0}$ are the positive-, negative- and zero- sequence current of phase *A*;
p is the fault distance expressed in per-unit (p.u.); and
$\mathbf{Z_{L1}}$, $\mathbf{Z_{L2}}$ and $\mathbf{Z_{L0}}$ are the positive-, negative- and zero-sequence impedances of the protected line.

Polarizing the first equation with the positive-sequence current without the pre-fault positive current and taking its imaginary part, the fault resistance in the positive-sequence branch is eliminated as is shown in (3).

$$\begin{aligned}\Delta \boldsymbol{I_1}^* \cdot (\mathbf{V_1} - \mathbf{I_1} \cdot p \cdot \mathbf{Z_{L1}} - \mathbf{I_1} \cdot R_{FB}) \\ = \Delta \boldsymbol{I_1}^* \cdot (\mathbf{V_2} - \mathbf{I_2} \cdot p \cdot \mathbf{Z_{L2}} - \mathbf{I_2} \cdot R_{FB})\end{aligned} \tag{3}$$

where $\mathbf{\Delta I_1}$ is the positive-sequence current without the prefault current.

Taking the imaginary part:

$$Imag[\Delta\mathbf{I_1}^* \cdot (\mathbf{V_1} - \mathbf{I_1} \cdot p \cdot \mathbf{Z_{L1}} - \mathbf{I_1} \cdot R_{FB})] = Imag[\Delta\mathbf{I_1}^* \cdot (\mathbf{V_2} - \mathbf{I_2} \cdot p \cdot \mathbf{Z_{L2}} - \mathbf{I_2} \cdot R_{FB})] \quad (4)$$

$$Imag[\Delta\mathbf{I_1}^* \cdot (\mathbf{V_1} - \mathbf{I_1} \cdot p \cdot \mathbf{Z_{L1}})] = Imag[\Delta\boldsymbol{I_1}^* \cdot (\mathbf{V_2} - \mathbf{I_2} \cdot p \cdot \mathbf{Z_{L2}} - \mathbf{I_2} \cdot R_{FB})] \quad (5)$$

The fault distance is obtained by solving:

$$p = \frac{Imag[\Delta\mathbf{I_1}^* \cdot (\mathbf{V_1} - \mathbf{V_2})] + Imag[\Delta\mathbf{I_1}^* \cdot \mathbf{I_2} \cdot R_{FB}]}{Imag[\Delta\mathbf{I_1}^* \cdot (\mathbf{I_1} - \mathbf{I_2}) \cdot \mathbf{Z_{L1}}]} \quad (6)$$

By polarizing the second equation with the zero-sequence current and taking its imaginary part, the fault resistance in the zero-sequence branch ($R_{FB} + 3R_G$) is eliminated:

$$Imag[\mathbf{I_0}^* \cdot (\mathbf{V_0} - \mathbf{I_0} \cdot p \cdot \mathbf{Z_{L0}})] = Imag[\mathbf{I_0}^* \cdot (\mathbf{V_2} - \mathbf{I_2} \cdot p \cdot \mathbf{Z_{L2}} - \mathbf{I_2} \cdot R_{FB})] \quad (7)$$

Solving for the fault distance yields:

$$p = \frac{Imag[\mathbf{I_0}^* \cdot (\mathbf{V_2} - \mathbf{V_0})] - Imag[\mathbf{I_0}^* \cdot \mathbf{I_2} \cdot R_{FB}]}{Imag[\mathbf{I_0}^* \cdot (\mathbf{I_2} \cdot \mathbf{Z_{L1}} - \mathbf{I_0} \cdot \mathbf{Z_{L0}})]} \quad (8)$$

This way, two equations (the equations (6) and (8)) and two unknowns (p and R_{FB}) are obtained. One of the unknowns is the per-unit fault distance, and the other is the fault resistance in the positive-sequence branch, which is equal to that of the negative-sequence branch. From these two equations, the per-unit fault distance can be determined.

The resulting expression for the fault distance is :

$$p = k_1 + k_2 \cdot R_{FB} \quad (9)$$

where:

$$k_1 = \frac{Imag[\Delta\mathbf{I_1}^* \cdot (\mathbf{V_1} - \mathbf{V_2})]}{Imag[\Delta\mathbf{I_1}^* \cdot (\mathbf{I_1} - \mathbf{I_2}) \cdot \mathbf{Z_{L1}}]}$$

$$k_2 = \frac{Imag[\Delta\mathbf{I_1}^* \cdot \mathbf{I_2}]}{Imag[\Delta\mathbf{I_1}^* \cdot (\mathbf{I_1} - \mathbf{I_2}) \cdot \mathbf{Z_{L1}}]}$$

$$R_{FB} = \frac{\left(\frac{Imag[\mathbf{I_0}^* \cdot (\mathbf{V_2} - \mathbf{V_0})]}{Imag[\mathbf{I_0}^* \cdot (\mathbf{I_2} \cdot \mathbf{Z_{L1}} - \mathbf{I_0} \cdot \mathbf{Z_{L0}})]} - \frac{Imag[\Delta\mathbf{I_1}^* \cdot (\mathbf{V_1} - \mathbf{V_2})]}{Imag[\Delta\mathbf{I_1}^* \cdot (\mathbf{I_1} - \mathbf{I_2}) \cdot \mathbf{Z_{L1}}]}\right)}{\left(\frac{Imag[\Delta\mathbf{I_1}^* \cdot \mathbf{I_2}]}{Imag[\Delta\mathbf{I_1}^* \cdot (\mathbf{I_1} - \mathbf{I_2}) \cdot \mathbf{Z_{L1}}]} + \frac{Imag[\mathbf{I_0}^* \cdot \mathbf{I_2}]}{Imag[\mathbf{I_0}^* \cdot (\mathbf{I_2} \cdot \mathbf{Z_{L1}} - \mathbf{I_0} \cdot \mathbf{Z_{L0}})]}\right)}$$

Taking the previously defined R_{FB} parameter as a reference, the ground-fault resistance value can be obtained as:

$$3 \cdot R_G = \frac{\mathbf{V_0} - \mathbf{V_2} + \mathbf{I_2} \cdot p \cdot \mathbf{Z_{L1}} - \mathbf{I_0} \cdot p \cdot \mathbf{Z_{L0}} - \mathbf{I_0} \cdot \mathrm{R_{FB}}}{\mathbf{I_0}} \quad (10)$$

The equations derived above are specifically applicable to a double phase-to-ground fault involving phases *B* and *C*. For a fault affecting phases *A* and *B*, the expressions must be adjusted by applying the appropriate phase-shift operators. Specifically, the positive-sequence quantities must be multiplied by the complex operator $\boldsymbol{a} = 1\angle 120°$, whereas the negative-sequence quantities must be multiplied by $\boldsymbol{a^2} = 1\angle 240°$. Consequently, the per-unit fault distance for a fault affecting phases *A* and *B* can be expressed in terms of the previously calculated expression as follows:

$$p = k_1 + k_2 \cdot R_{FB} \quad (11)$$

In this scenario, these components take the following values:

$$k_1 = \frac{Imag[(\Delta\mathbf{I_1} \cdot \mathbf{a})^* \cdot (\mathbf{V_1} \cdot \mathbf{a} - \mathbf{V_2} \cdot \mathbf{a^2})]}{Imag[(\Delta\mathbf{I_1} \cdot \mathbf{a})^* \cdot (\mathbf{I_1} \cdot \mathbf{a} - \mathbf{I_2} \cdot \mathbf{a^2}) \cdot \mathbf{Z_{L1}}]}$$

$$k_2 = \frac{Imag[(\Delta\boldsymbol{I_1} \cdot \mathbf{a})^* \cdot \boldsymbol{I_2} \cdot \mathbf{a^2}]}{Imag[(\Delta\boldsymbol{I_1} \cdot \mathbf{a})^* \cdot (\boldsymbol{I_1} \cdot \mathbf{a} - \boldsymbol{I_2} \cdot \mathbf{a^2}) \cdot \mathbf{Z_{L1}}]}$$

$$R_{FB} = \frac{\left(\frac{Imag[\mathbf{I_0}^* \cdot (\mathbf{V_2} \cdot \mathbf{a^2} - \mathbf{V_0})]}{Imag[\mathbf{I_0}^* \cdot (\mathbf{I_2} \cdot \mathbf{a^2} \cdot \mathbf{Z_{L1}} - \mathbf{I_0} \cdot \mathbf{Z_{L0}})]} - \frac{Imag[(\Delta\mathbf{I_1} \cdot \mathbf{a})^* \cdot (\mathbf{V_1} \cdot \mathbf{a} - \mathbf{V_2} \cdot \mathbf{a^2})]}{Imag[(\Delta\mathbf{I_1} \cdot \mathbf{a})^* \cdot (\mathbf{I_1} \cdot \mathbf{a} - \mathbf{I_2} \cdot \mathbf{a^2}) \cdot \mathbf{Z_{L1}}]}\right)}{\left(\frac{Imag[(\Delta\mathbf{I_1} \cdot \mathbf{a})^* \cdot \mathbf{I_2} \cdot \mathbf{a^2}]}{Imag[(\Delta\mathbf{I_1} \cdot \mathbf{a})^* \cdot (\mathbf{I_1} \cdot \mathbf{a} - \mathbf{I_2} \cdot \mathbf{a^2}) \cdot \mathbf{Z_{L1}}]} + \frac{Imag[\mathbf{I_0}^* \cdot \mathbf{I_2} \cdot \mathbf{a^2}]}{Imag[\mathbf{I_0}^* \cdot (\mathbf{I_2} \cdot \mathbf{a^2} \cdot \mathbf{Z_{L1}} - \mathbf{I_0} \cdot \mathbf{Z_{L0}})]}\right)}$$

The ground-fault resistance value can be obtained as:

$$3 \cdot R_G = \frac{\mathbf{V_0} - \mathbf{V_2} \cdot \mathbf{a^2} + \mathbf{I_2} \cdot \mathbf{a^2} \cdot \mathrm{p} \cdot \mathbf{Z_{L1}} - \mathbf{I_0} \cdot \mathrm{p} \cdot \mathbf{Z_{L0}} - \mathbf{I_0} \cdot R_{FB}}{\mathbf{I_0}} \quad (12)$$

Similarly, for a double phase-to-ground fault involving phases *C* and *A*, the sequence quantities must be shifted accordingly. In this case, the positive-sequence quantities are multiplied by $\boldsymbol{a^2} = 1\angle 240°$ while the negative-sequence quantities are multiplied by $\boldsymbol{a} = 1\angle 120°$.

$$p = k_1 + k_2 \cdot R_{FB} \quad (13)$$

where:

$$k_1 = \frac{Imag[(\Delta\mathbf{I_1} \cdot \mathbf{a^2})^* \cdot (\mathbf{V_1} \cdot \mathbf{a^2} - \mathbf{V_2} \cdot \mathbf{a})]}{Imag[(\Delta\mathbf{I_1} \cdot \mathbf{a^2})^* \cdot (\mathbf{I_1} \cdot \mathbf{a^2} - \mathbf{I_2} \cdot \mathbf{a}) \cdot \mathbf{Z_{L1}}]}$$

$$k_2 = \frac{Imag[(\Delta\mathbf{I_1} \cdot \mathbf{a^2})^* \cdot \mathbf{I_2} \cdot \mathbf{a}]}{Imag[(\Delta\mathbf{I_1} \cdot \mathbf{a^2})^* \cdot (\mathbf{I_1} \cdot \mathbf{a^2} - \mathbf{I_2} \cdot \mathbf{a}) \cdot \mathbf{Z_{L1}}]}$$

$$R_{FB} = \frac{\left(\frac{Imag[\mathbf{I_0}^* \cdot (\mathbf{V_2} \cdot \mathbf{a} - \mathbf{V_0})]}{Imag[\mathbf{I_0}^* \cdot (\mathbf{I_2} \cdot \mathbf{a} \cdot \mathbf{Z_{L1}} - \mathbf{I_0} \cdot \mathbf{Z_{L0}})]} - \frac{Imag[(\Delta\mathbf{I_1} \cdot \mathbf{a^2})^* \cdot (\mathbf{V_1} \cdot \mathbf{a^2} - \mathbf{V_2} \cdot \mathbf{a})]}{Imag[(\Delta\mathbf{I_1} \cdot \mathbf{a^2})^* \cdot (\mathbf{I_1} \cdot \mathbf{a^2} - \mathbf{I_2} \cdot \mathbf{a}) \cdot \mathbf{Z_{L1}}]}\right)}{\left(\frac{Imag[(\Delta\mathbf{I_1} \cdot \mathbf{a^2})^* \cdot \mathbf{I_2} \cdot \mathbf{a}]}{Imag[(\Delta\mathbf{I_1} \cdot \mathbf{a^2})^* \cdot (\mathbf{I_1} \cdot \mathbf{a^2} - \mathbf{I_2} \cdot \mathbf{a}) \cdot \mathbf{Z_{L1}}]} + \frac{Imag[\mathbf{I_0}^* \cdot \mathbf{I_2} \cdot \mathbf{a}]}{Imag[\mathbf{I_0}^* \cdot (\mathbf{I_2} \cdot \mathbf{a} \cdot \mathbf{Z_{L1}} - \mathbf{I_0} \cdot \mathbf{Z_{L0}})]}\right)}$$

The ground-fault resistance value can be obtained as:

$$3 \cdot R_G = \frac{\mathbf{V_0} - \mathbf{V_2} \cdot \mathbf{a} + \mathbf{I_2} \cdot \mathbf{a} \cdot \mathrm{p} \cdot \mathbf{Z_{L1}} - \mathbf{I_0} \cdot \mathrm{p} \cdot \mathbf{Z_{L0}} - \mathbf{I_0} \cdot \mathrm{R_{FB}}}{\mathbf{I_0}} \quad (14)$$

C. Fault distance calculation with coupled sequence networks

In case the fault resistances of the involved phases are different,

$$R_{FB} \neq R_{FC}, \quad (15)$$

the sequence networks are coupled, and therefore phase-domain quantities must be used in this situation. The equations involved are the following:

$$\mathbf{V_b} = p \cdot [\mathbf{I_b} \cdot \mathbf{Z_S} + \mathbf{I_c} \cdot \mathbf{Z_M}] + \mathbf{I_b} \cdot R_{FB} + 3 \cdot \mathbf{I_0} \cdot R_G$$
$$\mathbf{V_c} = p \cdot [\mathbf{I_c} \cdot \mathbf{Z_S} + \mathbf{I_b} \cdot \mathbf{Z_M}] + \mathbf{I_c} \cdot R_{FC} + 3 \cdot \mathbf{I_0} \cdot R_G \quad (16)$$

Where the mutual impedance of the phase $\mathbf{Z_M}$, and the Self-impedance of the phase $\mathbf{Z_S}$ are shown in (17).

$$\mathbf{Z_M} = \frac{\mathbf{Z_{L0}} - \mathbf{Z_{L1}}}{3}$$

$$\mathbf{Z_S} = \frac{\mathbf{Z_{L0}} + 2 \cdot \mathbf{Z_{L1}}}{3} \tag{17}$$

By polarising the first equation with the prefault phase-*B* current and taking the imaginary part, the fault resistance R_{Fb} is removed from the expression. Consequently, the distance to the fault in per-unit terms is obtained in (18).

$$p = \frac{Imag[\Delta\mathbf{I_b}^{*}\cdot\mathbf{V_b}] - Imag[\Delta\mathbf{I_b}^{*}\cdot 3\cdot\mathbf{I_0}\cdot R_G]}{Imag[\Delta\mathbf{I_b}^{*}\cdot(\mathbf{I_b}\cdot\mathbf{Z_S}+\mathbf{I_c}\cdot\mathbf{Z_M})]} \tag{18}$$

By polarising the second equation with the prefault phase-*C* current and taking its imaginary component, the fault resistance R_{Fc} is removed from the expression. Accordingly, the distance to the fault in per-unit terms is given by (19).

$$p = \frac{Imag[\Delta\mathbf{I_c}^{*}\cdot\mathbf{V_c}] - Imag[\Delta\mathbf{I_c}^{*}\cdot 3\cdot\mathbf{I_0}\cdot R_G]}{Imag[\Delta\mathbf{I_c}^{*}\cdot(\mathbf{I_c}\cdot\mathbf{Z_S}+\mathbf{I_b}\cdot\mathbf{Z_M})]} \tag{19}$$

This way, two equations with two unknowns are obtained. The distance to the fault in the case of a *BCG* fault is therefore given by:

$$p = \frac{Imag[\Delta\mathbf{I_b}^{*}\cdot\mathbf{V_b}] - Imag[\Delta\mathbf{I_b}^{*}\cdot 3\cdot\mathbf{I_0}\cdot R_G]}{Imag[\Delta\mathbf{I_b}^{*}\cdot(\mathbf{I_b}\cdot\mathbf{Z_S}+\mathbf{I_c}\cdot\mathbf{Z_M})]} \tag{20}$$

where:

$$R_G = \frac{\left(\frac{Imag[\Delta\mathbf{I_b}^{*}\cdot\mathbf{V_b}]}{Imag[\Delta\mathbf{I_b}^{*}\cdot(\mathbf{I_b}\cdot\mathbf{Z_S}+\mathbf{I_c}\cdot\mathbf{Z_M})]}\right) - \left(\frac{Imag[\Delta\mathbf{I_c}^{*}\cdot\mathbf{V_c}]}{Imag[\Delta\mathbf{I_c}^{*}\cdot(\mathbf{I_c}\cdot\mathbf{Z_S}+\mathbf{I_b}\cdot\mathbf{Z_M})]}\right)}{\left(\frac{Imag[\Delta\mathbf{I_b}^{*}\cdot 3\cdot\mathbf{I_0}]}{Imag[\Delta\mathbf{I_b}^{*}\cdot(\mathbf{I_b}\cdot\mathbf{Z_S}+\mathbf{I_c}\cdot\mathbf{Z_M})]}\right) - \left(\frac{Imag[\Delta\mathbf{I_c}^{*}\cdot 3\cdot\mathbf{I_0}]}{Imag[\Delta\mathbf{I_c}^{*}\cdot(\mathbf{I_c}\cdot\mathbf{Z_S}+\mathbf{I_b}\cdot\mathbf{Z_M})]}\right)} \tag{21}$$

For an *ABG* fault:

$$p = \frac{Imag[\Delta\mathbf{I_a}^{*}\cdot\mathbf{V_a}] - Imag[\Delta\mathbf{I_a}^{*}\cdot 3\cdot\mathbf{I_0}\cdot R_G]}{Imag[\Delta\mathbf{I_a}^{*}\cdot(\mathbf{I_a}\cdot\mathbf{Z_S}+\mathbf{I_b}\cdot\mathbf{Z_M})]} \tag{22}$$

where:

$$R_G = \frac{\left(\frac{Imag[\Delta\mathbf{I_a}^{*}\cdot\mathbf{V_a}]}{Imag[\Delta\mathbf{I_a}^{*}\cdot(\mathbf{I_a}\cdot\mathbf{Z_S}+\mathbf{I_b}\cdot\mathbf{Z_M})]}\right) - \left(\frac{Imag[\Delta\mathbf{I_b}^{*}\cdot\mathbf{V_b}]}{Imag[\Delta\mathbf{I_b}^{*}\cdot(\mathbf{I_b}\cdot\mathbf{Z_S}+\mathbf{I_a}\cdot\mathbf{Z_M})]}\right)}{\left(\frac{Imag[\Delta\mathbf{I_a}^{*}\cdot 3\cdot\mathbf{I_0}]}{Imag[\Delta\mathbf{I_a}^{*}\cdot(\mathbf{I_a}\cdot\mathbf{Z_S}+\mathbf{I_b}\cdot\mathbf{Z_M})]}\right) - \left(\frac{Imag[\Delta\mathbf{I_b}^{*}\cdot 3\cdot\mathbf{I_0}]}{Imag[\Delta\mathbf{I_b}^{*}\cdot(\mathbf{I_b}\cdot\mathbf{Z_S}+\mathbf{I_a}\cdot\mathbf{Z_M})]}\right)} \tag{23}$$

Finally, for a *CAG* fault:

$$p = \frac{Imag[\Delta\mathbf{I_c}^{*}\cdot\mathbf{V_c}] - Imag[\Delta\mathbf{I_c}^{*}\cdot 3\cdot\mathbf{I_0}\cdot R_G]}{Imag[\Delta\mathbf{I_c}^{*}\cdot(\mathbf{I_c}\cdot\mathbf{Z_S}+\mathbf{I_a}\cdot\mathbf{Z_M})]} \tag{24}$$

where:

$$R_G = \frac{\left(\frac{Imag[\Delta\mathbf{I_c}^{*}\cdot\mathbf{V_c}]}{Imag[\Delta\mathbf{I_c}^{*}\cdot(\mathbf{I_c}\cdot\mathbf{Z_S}+\mathbf{I_a}\cdot\mathbf{Z_M})]}\right) - \left(\frac{Imag[\Delta\mathbf{I_a}^{*}\cdot\mathbf{V_a}]}{Imag[\Delta\mathbf{I_a}^{*}\cdot(\mathbf{I_a}\cdot\mathbf{Z_S}+\mathbf{I_a}\cdot\mathbf{Z_M})]}\right)}{\left(\frac{Imag[\Delta\mathbf{I_c}^{*}\cdot 3\cdot\mathbf{I_0}]}{Imag[\Delta\mathbf{I_a}^{*}\cdot(\mathbf{I_c}\cdot\mathbf{Z_S}+\mathbf{I_a}\cdot\mathbf{Z_M})]}\right) - \left(\frac{Imag[\Delta\mathbf{I_a}^{*}\cdot 3\cdot\mathbf{I_0}]}{Imag[\Delta\mathbf{I_a}^{*}\cdot(\mathbf{I_a}\cdot\mathbf{Z_S}+\mathbf{I_c}\cdot\mathbf{Z_M})]}\right)} \tag{25}$$

In the case of a *BCG* fault, the earth resistance is given by:

$$R_G = \frac{\left(\frac{Imag[\Delta\mathbf{I_b}^{*}\cdot\mathbf{V_b}]}{Imag[\Delta\mathbf{I_b}^{*}\cdot(\mathbf{I_b}\cdot\mathbf{Z_S}+\mathbf{I_c}\cdot\mathbf{Z_M})]}\right) - \left(\frac{Imag[\Delta\mathbf{I_c}^{*}\cdot\mathbf{V_c}]}{Imag[\Delta\mathbf{I_c}^{*}\cdot(\mathbf{I_c}\cdot\mathbf{Z_S}+\mathbf{I_b}\cdot\mathbf{Z_M})]}\right)}{\left(\frac{Imag[\Delta\mathbf{I_b}^{*}\cdot 3\cdot\mathbf{I_0}]}{Imag[\Delta\mathbf{I_b}^{*}\cdot(\mathbf{I_b}\cdot\mathbf{Z_S}+\mathbf{I_c}\cdot\mathbf{Z_M})]}\right) - \left(\frac{Imag[\Delta\mathbf{I_c}^{*}\cdot 3\cdot\mathbf{I_0}]}{Imag[\Delta\mathbf{I_c}^{*}\cdot(\mathbf{I_c}\cdot\mathbf{Z_S}+\mathbf{I_b}\cdot\mathbf{Z_M})]}\right)} \tag{26}$$

Phase *B* and *C* resistances are:

$$R_{FB} = \frac{\mathbf{V_b} - p\cdot[\mathbf{I_b}\cdot\mathbf{Z_S}+\mathbf{I_c}\cdot\mathbf{Z_M}] - 3\cdot\mathbf{I_0}\cdot R_G}{\Delta\mathbf{I_b}}$$

$$R_{FC} = \frac{\mathbf{V_c} - p\cdot[\mathbf{I_c}\cdot\mathbf{Z_S}+\mathbf{I_b}\cdot\mathbf{Z_M}] - 3\cdot\mathbf{I_0}\cdot R_G}{\Delta\mathbf{I_c}} \tag{27}$$

In the case of an *ABG* fault, the earth resistance is given by:

$$R_G = \frac{\left(\frac{Imag[\Delta\mathbf{I_a}^{*}\cdot\mathbf{V_a}]}{Imag[\Delta\mathbf{I_a}^{*}\cdot(\mathbf{I_a}\cdot\mathbf{Z_S}+\mathbf{I_b}\cdot\mathbf{Z_M})]}\right) - \left(\frac{Imag[\Delta\mathbf{I_b}^{*}\cdot\mathbf{V_b}]}{Imag[\Delta\mathbf{I_b}^{*}\cdot(\mathbf{I_b}\cdot\mathbf{Z_S}+\mathbf{I_a}\cdot\mathbf{Z_M})]}\right)}{\left(\frac{Imag[\Delta\mathbf{I_a}^{*}\cdot 3\cdot\mathbf{I_0}]}{Imag[\Delta\mathbf{I_a}^{*}\cdot(\mathbf{I_a}\cdot\mathbf{Z_S}+\mathbf{I_b}\cdot\mathbf{Z_M})]}\right) - \left(\frac{Imag[\Delta\mathbf{I_b}^{*}\cdot 3\cdot\mathbf{I_0}]}{Imag[\Delta\mathbf{I_b}^{*}\cdot(\mathbf{I_b}\cdot\mathbf{Z_S}+\mathbf{I_a}\cdot\mathbf{Z_M})]}\right)} \tag{28}$$

Phase *A* and *B* resistances are shown in (29).

$$R_{FA} = \frac{\mathbf{V_a} - p\cdot[\mathbf{I_a}\cdot\mathbf{Z_S}+\mathbf{I_b}\cdot\mathbf{Z_M}] - 3\cdot\mathbf{I_0}\cdot R_G}{\Delta\mathbf{I_a}}$$

$$R_{FB} = \frac{\mathbf{V_b} - p\cdot[\mathbf{I_b}\cdot\mathbf{Z_S}+\mathbf{I_a}\cdot\mathbf{Z_M}] - 3\cdot\mathbf{I_0}\cdot R_G}{\Delta\mathbf{I_b}} \tag{29}$$

In the case of an *CAN* fault, the earth resistance is given by (30).

$$R_G = \frac{\left(\frac{Imag[\Delta\mathbf{I_c}^{*}\cdot\mathbf{V_c}]}{Imag[\Delta\mathbf{I_c}^{*}\cdot(\mathbf{I_c}\cdot\mathbf{Z_S}+\mathbf{I_a}\cdot\mathbf{Z_M})]}\right) - \left(\frac{Imag[\Delta\mathbf{I_a}^{*}\cdot\mathbf{V_a}]}{Imag[\Delta\mathbf{I_a}^{*}\cdot(\mathbf{I_a}\cdot\mathbf{Z_S}+\mathbf{I_a}\cdot\mathbf{Z_M})]}\right)}{\left(\frac{Imag[\Delta\mathbf{I_c}^{*}\cdot 3\cdot\mathbf{I_0}]}{Imag[\Delta\mathbf{I_a}^{*}\cdot(\mathbf{I_c}\cdot\mathbf{Z_S}+\mathbf{I_a}\cdot\mathbf{Z_M})]}\right) - \left(\frac{Imag[\Delta\mathbf{I_a}^{*}\cdot 3\cdot\mathbf{I_0}]}{Imag[\Delta\mathbf{I_a}^{*}\cdot(\mathbf{I_a}\cdot\mathbf{Z_S}+\mathbf{I_c}\cdot\mathbf{Z_M})]}\right)} \tag{30}$$

Phase *C* and *A* resistances are shown in (31).

$$R_{FC} = \frac{V_c - p\cdot[\mathbf{I_c}\cdot\mathbf{Z_S}+\mathbf{I_a}\cdot\mathbf{Z_M}] - 3\cdot\mathbf{I_0}\cdot R_G}{\Delta\mathbf{I_c}}$$

$$R_{FA} = \frac{\mathbf{V_a} - p\cdot[\mathbf{I_a}\cdot\mathbf{Z_S}+\mathbf{I_c}\cdot\mathbf{Z_M}] - 3\cdot\mathbf{I_0}\cdot R_G}{\Delta\mathbf{I_a}} \tag{31}$$

The method based on phase currents is valid for both coupled and decoupled systems, whereas the sequence-based method is only applicable when two phase resistances are equal. Since the value of the phase resistance is unknown, the phase-current-based method is the appropriate choice.

3. Study cases

This section demonstrates the validity of the proposed distance algorithm for double phase-to-earth faults. This way, it includes the performed simulations, together with the analysis of a real field fault.

A. Simulations with MATLAB

Fig. 3 shows the MATLAB model used in the study cases.

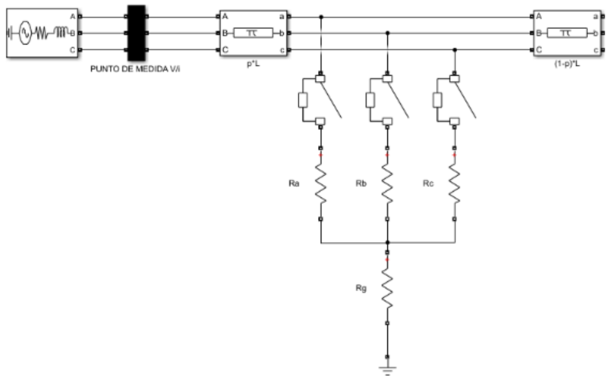

Fig. 3. MATLAB model

The model consists of a radial system where the system voltage is 25kV, the evaluated lines length L is 100 km and the line parameters of the protected line are as follows:

$$\mathbf{Z_{L1}} = 1.273 + 29.333\mathrm{j}\ \Omega$$
$$\mathbf{Z_{L0}} = 38.64 + 129.635\mathrm{j}\ \Omega$$

The short circuit power of the system equals to:

$$S_{CC} = 2000\ \mathrm{MVA}$$

The X/R ratio of the source impedance equals to:

$$X/_R = 7$$

The algorithm has been tested against multiple scenarios. However, due to space limitations, this section includes only one fault of each type, *ABG*, *BCG* and *CAG*, considering different fault resistances. Table I includes the analysed cases, phase-to-phase faults involving ground with different fault resistances. As shown in all cases, the distance estimation is highly accurate for both the distance and the ground resistance calculation. The phase resistance calculation also exhibits a very low, remaining below 2%. The results have been compared to traditional negative sequence polarization algorithm [1]. In the latter case, the error in distance calculation increases significantly ranging from 7 to 24.86 %, while the resistance estimation error is much higher and does not distinguish between the phases and ground resistance. These results confirm the robustness and reliability of the proposed algorithm.

Table I. – Fault cases.

FAULT TYPE	***ABG***	***BCG***	***CAG***
Real fault distance (p.u.)	0.35	0.55	0.75
Calculated fault distance with traditional I2 polarization (p.u.)	0.437	0.51	0.69
Traditional polarization error (%)	24.86	-7.27	-8
Calculated fault distance with proposed methodology (p.u.)	0.35	0.55	0.75
Proposed methodology error (%)	0	0	0
Real R_A (Ω)	5	∞	10
Calculated R_A (Ω)	5.01	∞	10.01
Real R_B (Ω)	8	3	∞
Calculated R_B (Ω)	8.01	3.01	∞
Real R_C (Ω)	∞	1	10
Calculated R_C (Ω)	∞	1.01	10.01
Proposed methodology $R_{A\text{-}B\text{-}C}$ error (%)	0.2	1	0.1
Real R_g (Ω)	16	1	2
Calculated R_g (Ω)	16	1	2
Proposed methodology R_g error (%)	0	0	0
Calculated R traditional method (Ω)	6.47	2.14	10.2

The tests performed correspond to ideal operating conditions, without prefault current and assuming perfectly known line parameters. Under these circumstances, the proposed method yields very small errors in the estimation of Rg, the remaining resistances, and the fault distance. However, in real power systems, several non-ideal factors must be considered. Parameter uncertainties, such as deviations in line impedances, mutual coupling effects, or conductor temperature, together with CT and VT ratio and phase-angle errors, inevitably introduce inaccuracies in the measured phasors. In addition, the presence of prefault load current modifies the voltage and current relationships used by the algorithm, which can further affect the estimation process.

Despite these sources of uncertainty, the proposed phase-current-based method is expected to remain significantly more robust than traditional approaches. Classical negative-sequence or sequence-component-based algorithms are particularly sensitive to parameter mismatch, since they rely on assumptions such as equal phase resistances and balanced prefault conditions. When these assumptions are not satisfied, as typically occurs under real-world operating conditions, the error increases substantially. This sensitivity explains why traditional methods exhibit notably larger deviations in both distance and resistance estimation, whereas the proposed method maintains a considerably higher degree of accuracy and discrimination capability

B. Real Field Fault

To validate the proposed fault distance calculation methodology, a real-world case study has been employed.

In Thailand, November 2025, a double phase-to-earth fault occurred when a network recloser failed in a radial distribution system. The incident took place at night, when the prefault current was negligible. The line length L was 1.95 km from the measurement point, which coincides with the fault location. The parameters of the protected line were as follows:

$$\mathbf{Z_{L1}} = 0.094 + 0.669\mathrm{j}\ \Omega$$
$$\mathbf{Z_{L0}} = 0.411 + 3.534\mathrm{j}\ \Omega$$

From these values, the self and mutual impedances of the line computed according to the methodology described in Section 2 (Equation 17), are given by:

$$\mathbf{Z_S} = \frac{\mathbf{Z_{L0}} + 2 \cdot \mathbf{Z_{L1}}}{3} = 0.2 + 1.624j\ \Omega$$
$$\boldsymbol{Z_M} = \frac{\boldsymbol{Z_{L0}} - \boldsymbol{Z_{L1}}}{\mathbf{3}} = 0.106 + 0.955j\ \Omega$$

The measured voltage and currents are:

$$\mathbf{V_A} = 18720\angle 103°\ \mathrm{V}$$
$$\mathbf{V_B} = 2564\angle -61°\ \mathrm{V}$$
$$\mathbf{V_C} = 2000\angle -126.22°\ \mathrm{V}$$
$$\mathbf{I_A} = 12.46\angle -178.44°\ \mathrm{A}$$
$$\mathbf{I_B} = 1632\angle -90.81°\ \mathrm{A}$$
$$\mathbf{I_C} = 1550\angle 152.93°\ \mathrm{A}$$
$$\mathbf{I_0} = 564.2\angle -146.8°\ \mathrm{A}$$

Using these values, the earth fault resistance is determined as follows:

$$R_G = \frac{\left(\frac{Imag[\Delta \mathbf{I_b}^{*} \cdot \mathbf{V_b}]}{Imag[\Delta \mathbf{I_b}^{*} \cdot (\mathbf{I_b} \cdot \mathbf{Z_S} + \mathbf{I_c} \cdot \mathbf{Z_M})]}\right) - \left(\frac{Imag[\Delta \mathbf{I_c}^{*} \cdot \mathbf{V_c}]}{Imag[\Delta \mathbf{I_c}^{*} \cdot (\mathbf{I_c} \cdot \mathbf{Z_S} + \mathbf{I_b} \cdot \mathbf{Z_M})]}\right)}{\left(\frac{Imag[\Delta \mathbf{I_b}^{*} \cdot 3 \cdot \mathbf{I_0}]}{Imag[\Delta \mathbf{I_b}^{*} \cdot (\mathbf{I_b} \cdot \mathbf{Z_S} + \mathbf{I_c} \cdot \mathbf{Z_M})]}\right) - \left(\frac{Imag[\Delta \mathbf{I_c}^{*} \cdot 3 \cdot \mathbf{I_0}]}{Imag[\Delta \mathbf{I_c}^{*} \cdot (\mathbf{I_c} \cdot \mathbf{Z_S} + \mathbf{I_b} \cdot \mathbf{Z_M})]}\right)} = 0.204\ \Omega$$

Phase-*B* and phase-*C* resistances are computed.

$$R_{FB} = \frac{\mathbf{V_b} - p \cdot [\mathbf{I_b} \cdot \mathbf{Z_S} + \mathbf{I_c} \cdot \mathbf{Z_M}] - 3 \cdot \mathbf{I_0} \cdot R_G}{\mathbf{I_b}} = 0.426\ \Omega$$

$$R_{FC} = \frac{\mathbf{V_c} - p \cdot [\mathbf{I_c} \cdot \mathbf{Z_S} + \mathbf{I_b} \cdot \mathbf{Z_M}] - 3 \cdot \mathbf{I_0} \cdot R_G}{\mathbf{I_c}} = 0.729\ \Omega$$

Finally, the distance to the fault is calculated.

$$p = \frac{Imag[\Delta\mathbf{I_b}^* \cdot \mathbf{V_b}] - Imag[\Delta\mathbf{I_b}^* \cdot 3 \cdot \mathbf{I_0} \cdot R_g]}{Imag[\Delta\mathbf{I_b}^* \cdot (\mathbf{I_b} \cdot \mathbf{Z_S} + \mathbf{I_c} \cdot \mathbf{Z_m})]} = 0.944\ p.u.$$

$$d = p \cdot L = 1.84\ km$$

The resulting error is 110 metres, which represents a 5.64 %. Given the short length of the line, the calculated fault distance can be considered accurate. All computed resistances are purely real, and therefore they can be regarded as correct.

4. Conclusions

This paper has introduced a new algorithm for locating double phase-to-earth faults and for estimating the associated fault resistances, considering both scenarios in which the phase fault resistances are equal and those where they differ.
Given the solid theoretical foundation of the equations employed, both the simulations carried out and the analysis of the real field fault yield highly satisfactory results in estimating the fault distance as well as the phase and earth resistances. This achievement represents a significant improvement in the treatment of double phase-to-earth faults, reinforcing the robustness and practical applicability of the proposed distance algorithm.
The present study has been conducted under ideal assumptions, without prefault load and with nominal line parameters; therefore, a full evaluation under non-ideal conditions remains necessary. These considerations define the scope and limitations of the current analysis and highlight the need for extended validation in realistic system settings. Overall, the proposed method provides a more reliable and resilient estimation framework, particularly when confronted with non-ideal factors such as line-parameter mismatch and instrument-transformer errors. Traditional algorithms show significantly greater sensitivity to these effects, which reinforces the methodological benefits and practical applicability of the proposed solution.
Further work will include the analysis of additional fault types, particularly phase-to-ground and three-phase faults, in order to confirm the robustness and general applicability of the proposed method across a broader set of real-world scenarios. The computational complexity of the proposed method is low enough to enable real-time execution, making it suitable for implementation in digital protection platforms. As a future development, the algorithm can be deployed and validated in an RTDS environment to assess its performance under real-time constraints.

Acknowledgement

The authors gratefully acknowledge GISEL Research Group (IT1799-26) and ELEKTRIKER Research Group (IT1647-22).

References

[1] Ziegler G. "Numerical distance protection. Principles and applications," 4th ed. Publicis Erlangen, 2011.
[2] J. L. Blackburn and T. J. Domin, "Protective Relaying: Principles and Applications," 5th ed. CRC Press, 2024.
[3] IEEE Power and Energy Society, "IEEE Guide for Protective Relay Applications to Transmission Lines," *IEEE Std C37.113-2025*.
[4] M. G. Adamiak and B. Kasztenny, "Next-Generation Distance Protection: Challenges and Trends," *IEEE Power and Energy Magazine*, vol. 22, no. 2, 2024.
[5] S. Azizi et al., "A Review on Fault Location Methods in Resilient Power Grids," *IEEE Access*, vol. 11, 2023.
[6] H. Miller and J. Burger, "Impact of High-Resistance Faults on Distance Elements in Radial Systems," *IEEE Transactions Power Delivery*, vol. 38, no. 4, 2023.
[7] Y. Zhong, X. Kang, Z. Jiao, Z. Wang and J. Suonan, "A Novel Distance Protection Algorithm for the Phase-Ground Fault," *IEEE Transactions Power Delivery*, vol. 29, no. 4, pp. 1718-1725, Aug. 2014
[8] L. Zhang et al., "Improved Distance Protection for Lines with Heavy Infeed and High Fault Resistance," *Electr. Power Syst. Res.*, vol. 214, 2023.
[9] P. Kundu, "Advanced Sequence-Domain Analysis for Asymmetrical Faults," *IEEE Transactions Smart Grid*, vol. 14, no. 1, 2023.
[10] J. J. Roberts, "Limitations of Conventional Fault Loops in 2LG Fault Scenarios," *IET Generation Transmission Distribution*, vol. 18, no. 3, 2024.
[11] K. Chen et al., "Deep Learning-based Fault Distance Estimation for Double-End-Fed Lines," *IEEE Transaction Industry Inform.*, vol. 19, 2024.
[12] R. G. Smith, "Dynamic Apparent Impedance Trajectories during Double Phase-to-Ground Events," *Power Syst. Technol.*, 2025.
[13] Y. Liang, Z. Lu, W. Li, W. Zha and Y. Huo, "A Novel Fault Impedance Calculation Method for Distance Protection Against Fault Resistance," *IEEE Transactions Power Delivery*, vol. 35, no. 1, pp. 396-407, Feb. 2020,
[14] X. Wang and Y. Liu, "A Novel Phase-Domain Algorithm for Fault Location in Unbalanced Networks," *IEEE Transactions Power Delivery.*, vol. 39, no. 2, 2024.
[15] M. Silva and P. Costa, "Decoupling Sequence Networks for Unequal Phase Resistances," *Int. J. Electric Power Energy Systems*, vol. 155, 2025.
[16] M. M. Eissa, "Ground distance relay Compensation based on fault resistance calculation," in *IEEE Transactions Power Delivery*, vol. 21, no. 4, pp. 1830-1835, 2006.
[17] A. S. Al-Rashidi, "Accurate Resistance Estimation in 2LG Faults using Synchrophasor Measurements," *Electric Power Components and Systems*, 2024.
[18] F. Jimenez and A. Gomez, "Complex Operator Application for Phase-Shift Correction in Distance Relays," *IEEE Transactions Instrum. Meas.*, vol. 73, 2024.
[19] T. Nguyen, "Stability of Distance Protection under Non-Homogeneous Line Parameters," *Energies*, vol. 17, no. 5, 2024.
[20] B. Wright, "Impact of Grounding Resistance on 2LG Fault Loop Accuracy," *Journal of Modern Power Systems and Clean Energy*, 2025.
[21] L. M. Fernandez, "Enhanced Fault Location for Radial Systems via Sequence Network Analysis," *IEEE PES General Meeting*, 2025.